IEEE Photonics Journal
An IEEE Photonics Society Publication

Sensitivity Enhancement of Ultrahigh-Order Mode Based Magnetic Field Sensor via Vernier Effect and Coarse Wavelength Sampling

Volume 13, Number 3, June 2021

Wenbin Lin
Yingcong Zhang
Wenjun Cai
Kaihong Zhang
Xianping Wang
Cheng Yin
Wen Yuan
Minghuang Sang

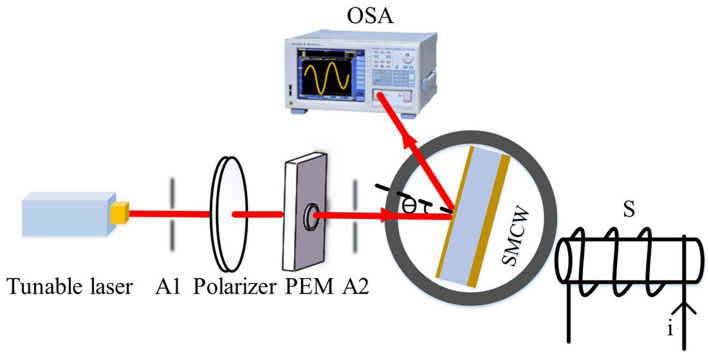

DOI: 10.1109/JPHOT.2021.3087255

Sensitivity Enhancement of Ultrahigh-Order Mode Based Magnetic Field Sensor via Vernier Effect and Coarse Wavelength Sampling

Wenbin Lin,[1] Yingcong Zhang,[1] Wenjun Cai,[1] Kaihong Zhang,[1] Xianping Wang,[1] Cheng Yin,[2] Wen Yuan,[1] and Minghuang Sang[1]

[1]Jiangxi Key Laboratory of Photoelectronics and Telecommunication, College of Physics and Communication Electronics, Jiangxi Normal University, Nanchang 330022, China
[2]Jiangsu Key Laboratory of Power Transmission and Distribution Equipment Technology, Hohai University, Changzhou 213022, , China

DOI:10.1109/JPHOT.2021.3087255

Manuscript received April 14, 2021; revised May 22, 2021; accepted June 3, 2021. Date of publication June 14, 2021; date of current version July 26, 2021. This work was supported in part by the National Natural Science Foundation of China under Grants 12064017, 61765008, 11864017, 11764020, 11804133, and 51567011, and in part by the Open Fund by State Key Laboratory of Advanced Optical Communication Systems and Networks under Grant 2017GZKF18. Corresponding author: Xianping Wang (e-mail: xpwangphysics@gmail.com).

Abstract: A methodology combining the asymmetrical metal-cladding waveguide (aSMCW) excited ultrahigh-order modes and coarse wavelength induced Vernier effect is theoretically proposed to enhance the sensitivity of the magnetic field sensor. In our aSMCW structure, a transparent glass SF11 with a sub-millimeter scale thickness is selected as the guiding layer, whose magnetically modulated refractive index leads to a variation of resonant wavelength. By controlling the sampling interval of tunable laser, the Vernier effect assisted resonant wavelength shift is more distinguishable and the sensitivity is enhanced about 20 times. Our sensitivity enhancement method is low cost since the optical spectrum analyzer (OSA) with a fine resolution is needless.

Index Terms: Sensor systems, optical waveguides, physical optics.

1. Introduction

Magnetic field sensors are significant devices in many monitoring applications, ranging from navigation [1], positioning [2] to geophysical explorations [3]. Naturally, variety of technologies are proposed to realize magnetic field detection. The utilize of the magnetically sensitive material to induce transformation of the variation of the magnetic field to other easy-measured physical quantities is a well-researched method. For example, the combination of the magnetic fluid (MF) with all-optical fiber systems [4], [5] is to substitute the measurement of magnetic field to refractive index of the MF, the Faraday-effect based sensor can transform the variation of magnetic field to a change in the characteristic of light propagating [6], magnetoresistance based sensor [7], and magnetostriction based sensor [8]. Actually, these methodologies are highly related to the materials that used in the systems. Recently, the requirements for high precision in magnetic field sensors attract many attentions and numerous researches are proposed to enhance the sensitivity of the sensors, such as the lowering linear birefringence [9] and using the microfiber coupling structures

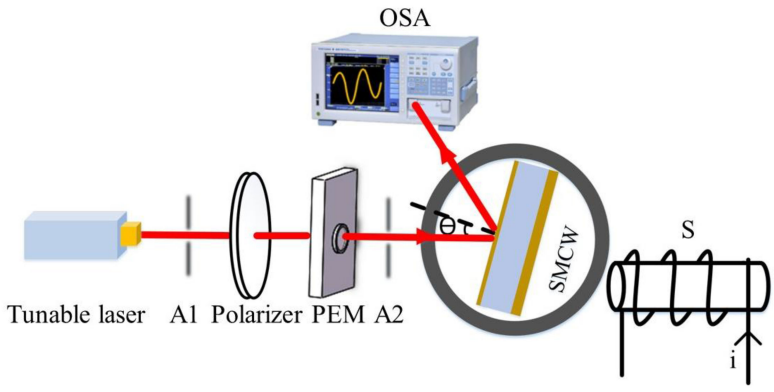

Fig.1. Schematic diagram of the magnetic field sensor.

[10]. These approaches can improve the sensitivity of the sensors by modifying the structures. To simplify the devices, Vernier effect can be harnessed in the sensor systems.

Vernier effect is a common technology that has been widely used in calipers and barometers. For these tools, the Vernier effect amplifies the small length difference to the sub ruler scale, which assists the realization of the length measurement with high resolution. With this advantage, Vernier effect is exploited in optical systems. As for the application, the cascade of two resonance cavities or interferometers with similar free spectral ranges (FSRs) produces a superimposed spectrum. A new FSR, which is broader than the old one will be obtained with a periodic envelope in this new spectrum. Therefore, by detecting the new FSR, the sensitivity can be severalfold amplified. With this method, numerous optical sensing schemes are proposed [11], [12]. However, in the general case, another resonant cavity should be induced in systems for reference interferometry to generate the Vernier effect, which greatly complicates the structure. Here, an asymmetrical metal-cladding waveguide (aSMCW) based magnetic field sensor, which can transfer the magnetic field intensity measurement to resonant wavelength shift detection, is proposed. Moreover, sampling Vernier effect is exploited in the system. Different sampling intervals for wavelength scanning by controlling the tunable laser can induce the Vernier effect and optimize the reflectivity spectrum. By means of this, the sensor structure can be greatly simplified and the sensitivity can be controlled and improved. It is believed that this method can be applied to other Vernier-effect based sensors, such as strain sensor [13], temperature sensor[14], [15], etc.

2. Device Structure and Sensing Principle

The schematic diagram of the magnetic field sensor is depicted in Fig. 1. A tunable laser provides a monochromatic light beam, whose wavelength is supposed to be λ. The light beam continuously passes through an aperture A1, whose diameter is 0.1 mm to collimate the beam, a polarization modulation system, another aperture with the same diameter A2, and then incident upon the top side of a classical aSMCW structure. The aSMCW is firmly mounted on a controllable $\theta/2\theta$ goniometer. An optical spectrum analyzer (OSA) is utilized to detect the reflected beam spectrum. The polarization modulation system consists of a polarizer and a photoelastic modulator (PEM), which assists the switch between left and the right circular polarizations of the incident beam. The aSMCW structure composes of a transparent glass SF11 layer sandwiched between a thin silver film on top and a thick silver slab underneath, and they serve as the guiding layer, the coupling layer, and the substrate, respectively. From top to bottom, their thicknesses are assumed as $h_1 = 20\,\text{nm}$, $h_2 = 0.8\text{mm}$, and $h_3 = 300\,\text{nm}$, respectively. The dielectric constant of the air is $\varepsilon_0 = 1$ and that of the silver can be described as $\varepsilon_1 = \varepsilon_3 = -125.35 + 12.555i$ [16]–[18]. For material SF11, the average refractive index is assumed as $n_2 = 1.77862$ with Verdet constant $V = 20\,\text{radT}^{-1}\text{m}^{-1}$ [19].

With the application of the free-space coupling technique [20], the incident beam can be directly coupled into the guiding layer. Moreover, the thickness of the guiding layer is of millimeter scale, which provides the condition for the excitation of ultrahigh-order modes (UHMs) and their dispersion equation can be simply approximated as [21]

$$\kappa_2 h_2 = m\pi, \tag{1}$$

where $\kappa_2 = k_0(\varepsilon_2 - N^2)^{1/2}$ and $m = 0, 1, 2, \ldots$is the mode order. Among them $k_0 = 2\pi/\lambda$ is the wavenumber with the wavelength λ in vacuum and $N = \sqrt{\varepsilon_0}\sin\theta_i$ is the effective refractive index at incident angle θ_i. According to transfer matrix method, the reflectivity coefficient of this employed aSMCW can be written as [22]

$$r_{0123} = \frac{r_{01} + r_{01}r_{12}r_{23}\exp(-2\alpha_2 h_2) + [r_{12} + r_{23}\exp(-2\alpha_2 h_2)]\exp(-2\alpha_1 h_1)}{1 + r_{12}r_{23}\exp(-2\alpha_2 h_2) + r_{01}[r_{12} + r_{23}\exp(-2\alpha_2 h_2)]\exp(-2\alpha_1 h_1)}, \tag{2}$$

where $\alpha_i = \sqrt{\beta^2 - k_0^2\varepsilon_i}$ is the attenuation coefficient and

$$r_{ij} = \begin{cases} \frac{k_i - k_j}{k_i + k_j} \text{ for TE polarization,} \\ \frac{k_i/\varepsilon_i - k_j/\varepsilon_j}{k_i/\varepsilon_i + k_j/\varepsilon_j} \text{ for TM polarization,} \end{cases} \tag{3}$$

is the Fresnel reflection coefficient at each interface. Among them β is the propagation constant, and the subscripts i, $j = 0 - 3$ refer to the air, thin silver layer, SF11 layer, and thick silver layer, respectively. Therefore, the reflectivity of the aSMCW can be acquired as $R = |r_{0123}|^2$.

For the employment of the SF11 glass as the guiding layer, the exertion of the current-induced magnetic field intensity B, which is parallel to the incident beam, leads to a medium circularly birefringent. The strength of the magnetic field B can be tuned by the current intensity. According to the previous research [19], the refractive indices of the left and right circularly polarized states of light can be given by

$$\begin{cases} n_2 = \frac{n_L + n_R}{2} \\ n_L = n_2 + \frac{VB\lambda}{2\pi} \\ n_R = n_2 - \frac{VB\lambda}{2\pi} \end{cases}, \tag{4}$$

respectively. Based on (1), (2), and (4), one can know that the aSMCW is polarization-independent [23] and the reflectivity spectrum of aSMCW for TE polarization (blue dot line) and TM polarization (red solid line) is depicted in Fig. 2(a). To clearly illustrate the result, two selected modes marked with a black dash box are enlarged and depicted in Fig. 2(b). For the simulation, the angle of incidence is fixed at $\theta_i = 6.172^\circ$, the amplitude of magnetic field is set as $B = 0$Gs, and the incident wavelength λ is tuned from 1535 nm to 1565 nm by a step of 0.006 nm. It can be seen from Fig. 2(a) and (b) that these two polarizations are overlapped with each other. Therefore, in the following simulation, TE polarization is selected for the simulation, while the TM polarization has the similar results.

Performing the differential operation over (1), the FSR can be calculated as [24]

$$FSR = \frac{\lambda^2}{2h_2\sqrt{n_2^2 - N^2}}. \tag{5}$$

Actually, with the operation of polarization modulation system, the monochromatic light beam from the tunable laser can be switched between the left and right circular polarization, and then couples into the aSMCW. Therefore, the UHMs, which have been demonstrated highly sensitive to the parameters of the structure and material [25], [26], will be excited. According to (4), when the amplitude of magnetic field B gradually increases, the resonant wavelength correspondingly shifts, due to the magnetic field intensity B leads to the variation of the n_L or n_R. Two modes that marked with a black dash box in Fig. 2(a) are selected and enlarged shown in Fig. 2(c) and (d) for detailed analysis. The Fig. 2(c) shows the situation where the incident beam is right circularly polarized

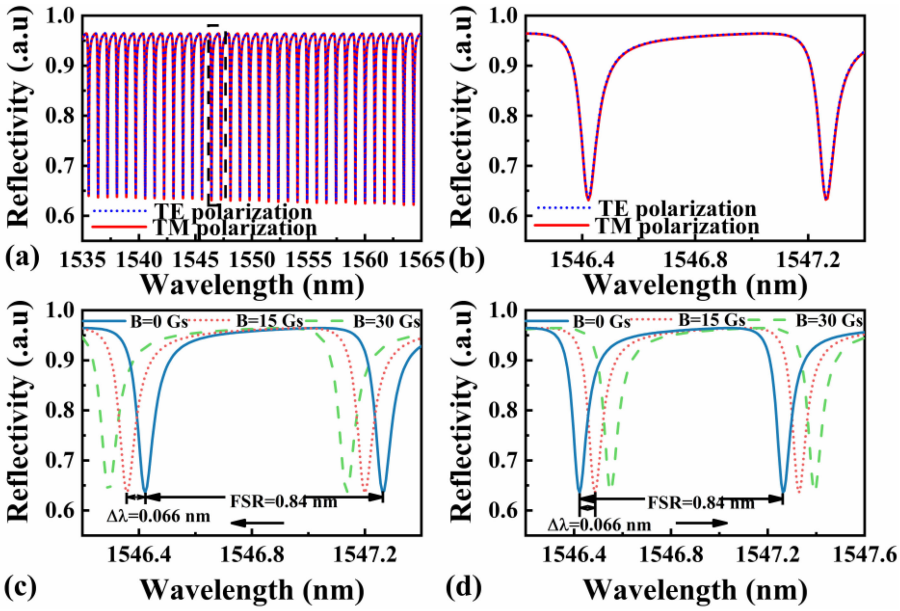

Fig, 2. (a) Reflectivity spectrum for TE polarization (blue dot line) and TM polarization (red solid line), (b) partial enlargement of picture (a); Reflectivity spectrum for (c) right circular polarization, and (d) left circular polarization at magnetic field intensity B = 0 Gs (blue solid line), B = 15 Gs (red dot line), and B = 30 Gs (green dash line), respectively.

state. It can be seen that when the amplitude of magnetic field B increases from 0 Gs to 30 Gs with a step size of 15 Gs, the resonant dips shift left, and the FSR is about 0.84 nm, which agree with the calculated result ($FSR = 0.845$ nm). The displacement of the resonant dip at wavelength $\sim$1546.4 nm is $\Delta\lambda = 0.066$ nm. The figure also shows that as the amplitude of magnetic field B equally increases, the displacement of the resonant wavelength correspondingly evenly grows. Thus, with this shift, the measurement of the magnetic field intensity can be transferred to the detection of the resonant wavelength shifts. For left circularly polarized state incident beam, the reflectivity spectrum portraited in Fig. 2(d). It can be found that with the enhancement of the magnetic field intensity, the resonant dips have a right shift, and the difference is $\Delta\lambda = 0.066$ nm at wavelength around $\sim$1546.4 nm. For both the left and right circularly polarization, the change of the magnetic field can cause the shift of the resonant dip, and the displacements of the resonant dip are nearly the same. Therefore, the following simulation is based on right circularly polarization, for the left circularly polarization will have the similar results.

3. Vernier Effect and Sensitivity Analysis

To induce the vernier effect, the incident wavelength λ is tuned from 1535 nm to 1565 nm by a step of 0.88 nm. This sampling interval is marginally greater than FSR of the low finesse sensor that discussed in section 2. Accordingly, a phase difference will exist between the incident beam wavelength and the low finesse sensor spectrum. As the wavelength increases, the phase difference will accumulate and when the phase difference varies 2π, the reflectivity will be the same. The sensitivity amplification factor is defined as [13]

$$M = \left| \frac{FSR}{FSR - SI} \right|, \tag{6}$$

where SI is sampling interval.

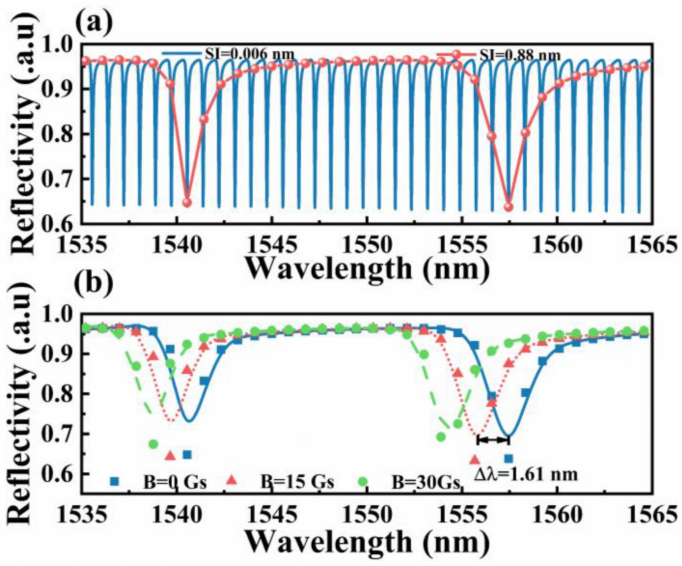

Fig. 3. Reflectivity spectrum for (a) $SI = 0.006$ nm (blue solid line) and $SI = 0.88$ nm (red line with circle symbol) and (b) $SI = 0.88$ nm at magnetic field intensity B = 0 Gs (blue square scatters), B = 15 Gs (red rectangle scatters), and B = 30 Gs (green circle scatters), and their fitting curve as blue solid line, red dot line, and green dash line, respectively.

According to (5) and (6), the theoretical sensitivity amplification factor for sampling interval $SI = 0.88$ nm is 24.71 times. Fig. 3(a) depicts the reflectivity spectrum with different wavelength sampling interval. The blue solid line represents the situation where the sampling interval is 0.006 nm while the red line with circle symbol represents the sampling interval is 0.88 nm. It can be seen that for sampling interval $SI = 0.88$ nm, the reflectivity spectrum only has two resonant dips when the wavelength ranges from 1535 nm to 1565 nm. The sampling interval $SI = 0.88$ nm at different magnetic field intensity is illustrated in Fig. 3(b). The blue square scatters, red rectangle scatters, and green circle scatters represent the condition where the amplitude of magnetic field is $B = 0$ Gs, $B = 15$ Gs, and $B = 30$ Gs, respectively. In order to improve the measurement accuracy, the smoothing spline fitting is employed to fit these scatters. The fitting results are also shown in Fig. 3(b) with the blue solid line, red dot line, and green dash line when the magnetic field intensity is $B = 0$ Gs, $B = 15$ Gs, and $B = 30$ Gs, respectively. It can be seen that resonant dips shift left and the displacement is $\Delta\lambda = 1.61$ nm. Compared to the low finesse sensor, this shift is more distinguishable and convenient to be detected. The simulated sensitivity amplification factor is 24.39 times, which has a good agreement with the theoretical calculation.

The spectrum shifts of different sampling intervals $SI = 0.006$ nm, $SI = 0.88$ nm, and $SI = 0.92$ nm as a function of the magnetic field intensity in the range of 0 Gs to 90 Gs are shown in Fig. 4. It is found that the wavelength shift and magnetic field intensity has a great linearity, which enables the sensing process. The sensitivity of different sampling intervals equal to their slopes, which are 0.0043 nm/Gs, 0.09 nm/Gs, and 0.06 nm/Gs, respectively. The sensitivity amplification factor for sampling intervals $SI = 0.88$ nm and $SI = 0.92$ nm are 22.12 times and 13.95 times, respectively. It exists a slight difference between the theoretical and simulated sensitivity amplification factor, which can be explained as following. During the process of the coarse wavelength sampling, the increment of the wavelength causes the variation of FSR, which is proved by (5), thus, FSR fluctuates with the mode order. Moreover, it can be found that the sensitivity for sampling intervals $SI = 0.88$ nm is larger than that of $SI = 0.92$ nm, and it can be explained by (6). It also worth noting that the selected sampling interval should merely be slightly larger than FSR, due to the fact that the large one will reduce the sensitivity, while the small one will not generate the Vernier effect. With the sensor utilizing the coarse wavelength sampling induced the Vernier effect, the resonant

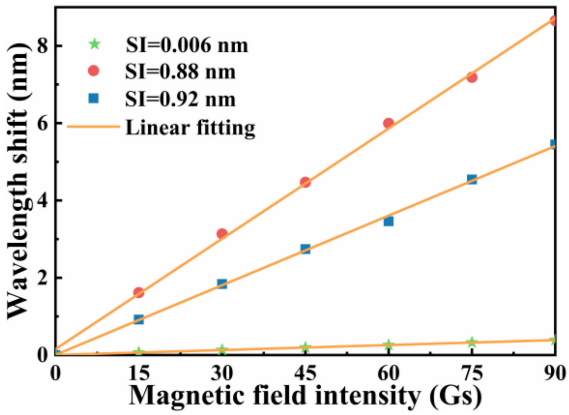

Fig. 4. Spectrum shifts of the different sampling intervals $SI = 0.006$ nm (green star scatters), $SI = 0.88$ nm (blue square scatters), and $SI = 0.92$ nm (red circle scatters) as a function of the magnetic field intensity in the range of 0 Gs to 90 Gs and their linear fitting results (orange solid line).

wavelength shifts are more discernable than that of the low fineness sensor. Therefore, while effectively improving the sensing accuracy, the sensor cost can also be generally cut in light of the fact that a fine OSA is no longer a necessary condition.

4. Conclusion

In summary, an aSMCW structure with inserting the SF11 glass as the guiding layer is presented to achieve the magnetic field intensity sensing by substituting the magnetic field intensity measurement to the detection of the resonant wavelength shift. The optimized Vernier-effect based sensitivity amplification method is proposed and utilized on sensor to improve the sensitivity. The results show that the sampling intervals that marginally greater than FSR effectively enhance the sensitivity up to 22.12 times and the simulating results are greatly agree with the theoretical results. In the practical application, it worth noting that to realize a higher sensitivity amplification factor, the selected sampling intervals should be properly adjusted to match the value of FSR. With this technique, the sensitivity of the magnetic field sensor can be controlled and improved, moreover, the cost of the sensor can be largely cut. It is believed that with these advantages, this method can be applied to other structures and the sensor can be widely utilized in sensor field.

References

[1] M. Y. Tkhorenko, B. V. Pavlov, E. V. Karshakov, and A. K. Volkovitsky, "On integration of a strapdown inertial navigation system with modern magnetic sensors," in *Proc. 25th Saint Petersburg Int. Conf. Integr. Navigation Syst.*, 2018, pp. 1–4.

[2] V. Pasku, A. D. Angelis, G. D. Angelis, A. Moschitta, and P. Carbone, "Magnetic field analysis for 3-D positioning applications," *IEEE Trans. Instrum. Meas.,* vol. 66, no. 5, pp. 935–943, May 2017.

[3] S. V. Poliakov, B. I. Reznikov, A. V. Shchennikov, E. A. Kopytenko, and B. V. Samsonov, "The range of induction-coil magnetic field sensors for geophysical explorations," *Seismic Instruments,* vol. 53, no. 1, pp. 1–18, 2017.

[4] R. Gao, Y. Jiang, and S. Abdelaziz, "All-fiber magnetic field sensors based on magnetic fluid-filled photonic crystal fibers," *Opt. Lett.,* vol. 38, no. 9, pp. 1539–1541, 2013.

[5] F. Wei *et al.*, "Magnetic field sensor based on a combination of a microfiber coupler covered with magnetic fluid and a sagnac loop," *Sci. Rep.,* vol. 7, no. 1, pp. 1–9, Jul. 2017.

[6] L. Cheng, J. Han, Z. Guo, L. Jin, and B.-O. Guan, "Faraday-rotation-based miniature magnetic field sensor using polarimetric heterodyning fiber grating laser," *Opt. Lett.,* vol. 38, no. 5, pp. 688–690, 2013.

[7] G. Kirat, O. Kizilaslan, and M. A. Aksan, "Magnetoresistance properties of magnetic Ni-Mn-Sn-B shape memory ribbons and magnetic field sensor aspects operating at room temperature," *J. Magnetism Magn. Mater.,* vol. 477, pp. 366–371, 2019.

[8] B. Wu *et al.*, "Magnetic field sensor based on a dual-frequency optoelectronic oscillator using cascaded magnetostrictive alloy-fiber Bragg grating-Fabry Perot and fiber Bragg grating-Fabry Perot filters," *Opt. Exp.,* vol. 26, no. 21, pp. 27628–27638, 2018.
[9] L. Cheng, J. Han, L. Jin, Z. Guo, and B. O. Guan, "Sensitivity enhancement of faraday effect based heterodyning fiber laser magnetic field sensor by lowering linear birefringence," *Opt Exp.,* vol. 21, no. 25, pp. 30156–30162, Dec. 2013.
[10] S. Pu, L. Mao, T. Yao, J. Gu, M. Lahoubi, and X. Zeng, "Microfiber coupling structures for magnetic field sensing with enhanced sensitivity," *IEEE Sensors J.,* vol. 17, no. 18, pp. 5857–5861, 2017.
[11] L. Jin, M. Li, and J. J. He, "Highly-sensitive silicon-oninsulator sensor based on two cascaded micro-ring resonators with vernier effect," in *Opt. Commun.*, vol. 284, no. 1, pp. 156–159, 2011.
[12] P. M. R. Robalinho, A. D. Gomes, and O. Frazão, "High enhancement strain sensor based on vernier effect using 2-fiber loop mirrors," *IEEE Photon. Technol. Lett.,* vol. 32, no. 18, pp. 1139–1142, Sep. 2020.
[13] Y. Wu, L. Xia, W. Li, and J. Xia, "Highly sensitive Fabry–Perot demodulation based on coarse wavelength sampling and vernier effect," *IEEE Photon. Technol. Lett.,* vol. 31, no. 6, pp. 487–490, Mar. 2019.
[14] Y. Yang *et al.*, "Sensitivity-enhanced temperature sensor by hybrid cascaded configuration of a sagnac loop and a F-P cavity," *Opt. Exp.,* vol. 25, no. 26, pp. 33290–33296, 2017.
[15] J. Zhang *et al.*, "Ultrasensitive temperature sensor with cascaded fiber optic Fabry–Perot interferometers based on vernier effect," *IEEE Photon. J.,* vol. 10, no. 5, Oct. 2018, Art. no. 6803411.
[16] P. B. Johnson and R. W. Christy, "Optical constants of the noble metals," *Phys. Rev. B,* vol. 6, no. 12, pp. 4370–4379, 1972.
[17] H. Wang, T. Tang, Z. Huang, J. Gong, and G. Jia, "Photonic spin hall effect modified by ultrathin au films and monolayer transition metal dichalcogenides in one-dimensional photonic crystal," *Plasmonics,* vol. 15, no. 6, pp. 2127–2135, 2020.
[18] G. Jia and C. Guo, "Interband-transition-modified third-order nonlinear optical properties of al nanoshells in carbon disulfide," *RSC Adv.,* vol. 6, no. 12, pp. 10038–10043, 2016, doi: 10.1039/C5RA25981A.
[19] R. Papukutty Rajan and A. Ghosh, "Enhancement of circular differential deflection of light in an optically active medium," *Opt. Lett.,* vol. 37, no. 7, pp. 1232–1234, 2012.
[20] H. Li, Z. Cao, H. Lu, and Q. Shen, "Free-space coupling of a light beam into a symmetrical metal-cladding optical waveguide," *Appl. Phys. Lett.,* vol. 83, no. 14, pp. 2757–2759, 2003.
[21] H. Lu, Z. Cao, H. Li, and Q. Shen, "Study of ultrahigh-order modes in a symmetrical metal-cladding optical waveguide," *Appl. Phys. Lett.,* vol. 85, no. 20, pp. 4579–4581, 2004.
[22] X. Liu, Z. Cao, P. Zhu, Q. Shen, and X. Liu, "Large positive and negative lateral optical beam shift in prism-waveguide coupling system," *Phys. Rev. E.,* vol. 73, no. 5, May 2006, Art. no. 056617.
[23] H. Li, Z. Cao, H. Lu, and Q. Shen, "Free-space coupling of a light beam into a symmetrical metal-cladding optical waveguide," *Appl. Phys. Lett.*, vol. 83, no. 14, pp. 2757–2759, 2003.
[24] H. Lu, Z. Cao, H. Li, Q. Shen, and X. Deng, "Polarization-independent and tunable comb filter based on a free-space coupling technique," *Opt. Lett.,* vol. 31, no. 3, pp. 386–388, 2006.
[25] X. Wang *et al.*, "High-sensitivity temperature sensor using the ultrahigh order mode-enhanced Goos-Hanchen effect," *Opt Exp.,* vol. 21, no. 11, pp. 13380–13385, Jun. 2013.
[26] Y. Wang, H. Li, Z. Cao, T. Yu, Q. Shen, and Y. He, "Oscillating wave sensor based on the Goos–Hänchen effect," *Appl. Phys. Lett.,* vol. 92, no. 6, 2008.